

# In-Medium Modifications of the $S_{11}(1535)$ Resonance and Eta Photoproduction

J. Lehr, M. Post and U. Mosel  
*Institut für Theoretische Physik, Universität Giessen*  
*D-35392 Giessen, Germany*  
(Dated: November 19, 2018)

We investigate the influence of possible in-medium modifications of the  $S_{11}(1535)$  in eta photoproduction in nuclei. Besides Fermi motion, Pauli blocking and binding effects also collisional broadening is accounted for. The in-medium width is obtained from a realistic resonance-hole model. Results on eta photoproduction are obtained from a semi-classical BUU transport model and compared with data. We find that calculations including a momentum dependent nucleon and resonance potential are in agreement with the recent KEK data. In contrast, collisional broadening has only little influence.

PACS numbers: 25.20.Lj, 25.20.x

## I. INTRODUCTION

Photon induced reactions on nuclei provide a promising tool for the investigation of in-medium properties of hadrons. However, the interpretation of data is often difficult, because it is hard to disentangle contributions from different resonances and/or different decay channels as e.g. in the case of pion production in the second resonance region. In this respect the study of the  $S_{11}(1535)$  is very interesting because of its strong coupling to  $N\eta$ . In the energy regime of  $E_\gamma \sim 600 - 900$  MeV this channel is strongly dominated by the  $S_{11}(1535)$  and therefore  $\eta$  photoproduction gives information almost solely about this resonance.

In the past, different experiments of  $\eta$  photoproduction on several nuclei (C, Al, Ca, Cu, Nb, Pb) were performed. The TAPS group covered the energy range from threshold up to photo energies of 800 MeV [1], whereas measurements at KEK [2, 3] provided data up to 1 GeV. Other theoretical approaches to the process discussed several in-medium effects. In [2] a QMD model was applied. Besides the trivial effects of Fermi motion and Pauli blocking, the authors found a strong influence due to collisional reactions of the  $S_{11}$ . The authors of [4] were able to describe the KEK data on Carbon under the assumption that both scalar and vector potential of the  $S_{11}$  vanish. However, the calculations were performed in nuclear matter and the  $\eta$  final state interactions were modelled by using a constant absorption factor. Hence, the findings of this work have to be checked by a more realistic model.

In this work, we calculate  $\eta$  photoproduction on different nuclei using a semi-classical BUU transport model, which was already successfully applied to the calculation of a variety of reactions (e.g. heavy-ion reactions [5], photon- and electron-induced reactions [6, 7]). Within this model,  $\eta$  photoproduction for energies up to 800 MeV was already addressed in [6, 8]. In contrast, we now want to extend our study to higher energies covered by the KEK data and to discuss medium modifications of the  $S_{11}$ . The  $S_{11}$  in-medium width is obtained from self-consistent resonance-hole calculations [9].

We start with a brief review of the BUU model and the implementation of the  $\eta$  and  $S_{11}$  dynamics in Sec. II followed by a discussion of in-medium modifications of the  $S_{11}$  width in Sec. III. In Sec. IV we show our results in comparison with experimental data.

## II. THE BUU MODEL

For the present studies, we use the BUU model reported in [7, 10]. The model is based upon a system of coupled BUU equations describing the evolution of the spectral distribution function  $F_i = \mathcal{A}_i f_i$  with the phase space density  $f_i$  of different particle types  $i = N, \pi, S_{11}(1535), \eta, \dots$ :

$$\left( \frac{\partial}{\partial t} + \vec{\nabla}_p H \cdot \vec{\nabla}_r - \vec{\nabla}_r H \cdot \vec{\nabla}_p \right) F_i(\vec{r}, \vec{p}, \mu; t) = \Sigma_i^< \mathcal{A}_i (1 - f_i(\vec{r}, \vec{p}, \mu; t)) - \Sigma_i^> \mathcal{A}_i f_i(\vec{r}, \vec{p}, \mu; t). \quad (1)$$

Here  $\mathcal{A}_i$  is the spectral function and  $H$  is a relativistic Hamilton function

$$H = \sqrt{(m + S)^2 + p^2} \quad (2)$$

with a scalar potential  $S$  described in Eq. (5).

$\Sigma_i^{\lessgtr}$  stand for the collision rates of particle species  $i$  and describe the gain and the loss of the distribution function at some 'point'  $(\vec{r}, \vec{p}, \mu, t)$  due to collisional reactions with particles of the same and other types. Therefore, the BUU equations are coupled via their right-hand sides. The set of equations is solved by a test particle ansatz for each density function  $F_i$ . For model details we refer the reader to [7, 10].

Besides the nucleon, our model contains 29 nucleon resonances with parameters taken from the analysis of Manley and Saleski [11] and all relevant mesonic degrees of freedom  $(\pi, \eta, \rho, \omega)$ . The  $\eta$  couples to the resonances  $S_{11}(1535)$ ,  $S_{11}(1650)$  and  $F_{17}(1990)$  with pole-mass branching ratios of 0.43, 0.03 and 0.94.

The single-particle energy of a nucleon in the local rest frame (LRF) of the surrounding nuclear matter is given by

$$\epsilon = \sqrt{(m_N - U_s)^2 + p_{\text{LRF}}^2} + U_0 \equiv \sqrt{m_N^2 + p_{\text{LRF}}^2} + V \quad (3)$$

with vector and scalar potentials  $U_0$  and  $U_s$ . For the nucleon, in the LRF the spatial components of the vector potential vanish in the mean-field approximation. In the non-relativistic limit,  $V$  corresponds to the difference of scalar and vector potential. For  $V$  we use the density and momentum dependent non-relativistic mean-field parametrization from Welke *et al.* [12]

$$V(\vec{r}, \vec{p}) = A \frac{\rho}{\rho_0} + B \left( \frac{\rho}{\rho_0} \right)^\tau + \frac{8C}{\rho_0} \int \frac{d^3 p'}{(2\pi)^3} \frac{\Theta(p_F(\rho(r)) - p')}{1 + \left( \frac{\vec{p} - \vec{p}'}{\Lambda} \right)^2}. \quad (4)$$

In this equation  $p_F = p_F(\rho)$  is the local Fermi momentum. We can work with a choice of parameter sets  $A, B, C, \tau, \Lambda$  determining the momentum dependence and stiffness of the nuclear matter equation of state (EOS) (cf. Table I). Here, we use either a momentum independent hard EOS (H) or a momentum dependent medium EOS (M). In Fig. 1 we show the momentum dependence of the potential  $V$  for the parameter set (M) for different densities.  $V$  is transformed in the LRF into a scalar potential  $S$  using

$$\sqrt{(m_N + S)^2 + p_{\text{LRF}}^2} = \sqrt{m_N^2 + p_{\text{LRF}}^2} + V. \quad (5)$$

We assume that the potential  $V$  for the  $S_{11}(1535)$  is also given by Eq. (4), and the scalar resonance potential  $S_R$  is obtained in the same way. The effective resonance mass is then given by

$$\mu_{\text{eff}} = \mu + S_R.$$

Since no detailed calculations exist for the  $S_{11}$ , this is a reasonable assumption.

### A. The elementary photon-nucleon reaction

The main source of  $\eta$  mesons is the elementary  $\gamma N$  reaction. It is known that in the threshold region the process  $\gamma p \rightarrow \eta p$  is well described by the excitation of the  $S_{11}$  resonance (see e.g. [13]). The contribution coming from the two other resonances coupling to  $N\eta$  are neglected, because the  $\eta N$  branching ratio of the  $S_{11}(1650)$  is very small and the  $F_{17}(1990)$  is beyond the considered energy range. Therefore, we use the following Breit-Wigner parametrization:

$$\begin{aligned} \sigma_{\gamma p \rightarrow S_{11} \rightarrow X} &= \left( \frac{k_0}{k} \right)^2 \frac{s \Gamma_\gamma(\sqrt{s}) \Gamma_{S_{11} \rightarrow X}(\sqrt{s})}{(s - M_{S_{11}}^2)^2 + s \Gamma_{S_{11} \rightarrow X}^2(\sqrt{s})} \frac{2m_N}{M_{S_{11}} \Gamma_0} |A_{1/2}^p|^2, \\ \sigma_{\gamma p \rightarrow S_{11} \rightarrow \eta p} &= \sigma_{\gamma p \rightarrow S_{11}} \frac{\Gamma_{S_{11} \rightarrow \eta p}(\sqrt{s})}{\Gamma_{S_{11} \rightarrow X}(\sqrt{s})} \end{aligned} \quad (6)$$

with  $\Gamma_\gamma = \Gamma_0 \cdot k/k_0$  [14] and the pole-mass decay width  $\Gamma_0 = 0.151$  GeV. The center of mass (cm) momentum  $k$  of the  $\gamma p$  pair depends on the cm energy  $\sqrt{s}$  (i.e. mass of the resonance),  $k_0 = k(M_{S_{11}})$  is the cm momentum taken at the pole mass of the  $S_{11}$ . The other (mass dependent) resonance widths  $\Gamma_{S_{11} \rightarrow X}$  and  $\Gamma_{S_{11} \rightarrow \eta N}$  are parametrized as in [10]. For the photocoupling helicity amplitude we use  $A_{1/2}^p = 0.109$  GeV $^{-1/2}$  [15]. The cross section for the reaction  $\gamma n \rightarrow S_{11}$  is obtained from (6) by

$$\sigma_{\gamma n} = \frac{2}{3} \sigma_{\gamma p}, \quad (7)$$

as suggested in [16], corresponding to  $A_{1/2}^n \sim 0.089$  GeV $^{-1/2}$ . This value results from a resonance fit to eta photo-production data on the deuteron and is connected to the value for  $A_{1/2}^p$  found in [15]. Therefore, we do not use the (smaller) values found in other analyses (e.g. [13]).

In Fig. 2 we show the cross section for the elementary process  $\gamma p \rightarrow \eta p$  in comparison with the data sets from [15, 17]. For energies up to  $E_\gamma \sim 1$  GeV the agreement with the data is good.

Our model also contains other channels for the elementary  $\gamma N$  interaction, namely  $\gamma N \rightarrow \pi N$ ,  $\pi\pi N$ ,  $P_{33}(1232)$ ,  $D_{13}(1520)$ ,  $F_{15}(1680)$ . These processes might also contribute to  $\eta$  photoproduction on nuclei via final state interactions (e.g. the reaction chain  $\gamma N \rightarrow \pi N$ ,  $\pi N \rightarrow S_{11} \rightarrow \eta N$ ). However, it was shown in [6] that they are rather small. The parametrization of these processes via resonance fits to experimental pion photoproduction data is similar to Eq. (6) and described in Ref. [6].

### B. Final state interactions

The  $\eta$  final state interactions (FSI) are assumed to be mediated by the re-excitation of resonances. In the energy range under consideration the  $S_{11}(1535)$  clearly dominates. The cross sections for elastic and inelastic  $\eta N$  reactions therefore are similar to Eq. (6) and strongly depend on the energy of the  $\eta$ :

$$\sigma_{\eta N \rightarrow S_{11} \rightarrow X} = \frac{4\pi}{p_{\eta N}^2} \frac{s\Gamma_{S_{11} \rightarrow \eta N}(\sqrt{s})\Gamma_{S_{11} \rightarrow X}(\sqrt{s})}{(s - M_{S_{11}}^2)^2 + s\Gamma_{S_{11} \rightarrow X}^2(\sqrt{s})} \quad (8)$$

with the  $\eta N$  cm momentum  $p_{\eta N}$ .  $X$  contains the decay channels  $N\pi$ ,  $N\eta$ ,  $N\rho$ ,  $N\sigma$  and  $P_{11}(1440)\pi$ . Among these,  $N\pi$  and  $N\eta$  are the relevant channels (branching ratio  $\sim 95\%$ ). In the medium, the  $S_{11}$  also undergoes FSI via the processes

$$\begin{aligned} NS_{11} &\leftrightarrow NN \\ NS_{11} &\rightarrow NS_{11} \\ NS_{11} &\leftrightarrow NR, R \neq S_{11}, \end{aligned} \quad (9)$$

which give rise to a finite collision width. This will be discussed in Sec. III. Of course, the absorption of  $S_{11}$  states in such reactions also contributes to the absorption of  $\eta$  mesons.

Finally, the coupled-channel treatment of our BUU model also allows for contributions from side-feeding reactions such as  $\pi N \rightarrow R \rightarrow \eta N$ . As already mentioned, the  $\eta$  mesons managing to escape the nucleus stem to a large extent from the elementary reaction chain  $\gamma N \rightarrow S_{11} \rightarrow N\eta$ .

### III. CALCULATION OF THE $S_{11}$ IN-MEDIUM WIDTH

In [18] the collisional broadening of the resonances  $P_{33}(1232)$ ,  $D_{13}(1520)$ ,  $S_{11}(1535)$  and  $F_{15}(1680)$  was calculated from the collision rates resulting from processes like (9):

$$\begin{aligned} \Sigma_{S_{11}N \rightarrow X}^>(E, p, \rho) &= \frac{1}{2E} \int \frac{d^3p_2}{(2\pi)^3} \frac{d\mu_2}{2E_2} \frac{d^3p_3}{(2\pi)^3} \frac{d\mu_3}{2E_3} \frac{d^3p_4}{(2\pi)^3} \frac{d\mu_4}{2E_4} (2\pi)^4 \delta^4(p + p_2 - p_3 - p_4) \\ &\times |\mathcal{M}_{S_{11}N \rightarrow X}|^2 \mathcal{A}_2 f_2 \mathcal{A}_3 (1 - f_3) \mathcal{A}_4 (1 - f_4) \end{aligned} \quad (10)$$

with  $X = NN$ ,  $S_{11}N$  and  $RN$ .  $f_2$  is the phase space density of the incoming nucleons,  $1 - f_{3,4}$  are the Pauli blocking factors for the outgoing particles included in the final state  $X$ . Note that such collision rates also appear in the collision integrals on the right-hand side of the BUU equations. Therefore, consistency between the collision widths and the processes explicitly included in the transport model is guaranteed. The matrix elements appearing in the collision rates are identical to those contained in the cross sections for the processes (9). Eq. (10) can be rearranged in the following way:

$$\Sigma^> = \rho_N \langle v_{\text{rel}}^{\text{cm}} \sigma_{S_{11}N \rightarrow X}^{\text{cm}} (1 - f_3)(1 - f_4) \rangle_N, \quad (11)$$

where the averaging is performed over the momentum distribution of the incoming nucleon and  $v_{\text{rel}}^{\text{cm}}$  is the relative velocity of the incoming  $S_{11}N$  pair in the cm frame. We see that this expression is similar to what one obtains from the low density theorem  $\Gamma_{\text{coll}} = \rho v \sigma_{\text{tot}}$ , leading to an increase of the collision rates with momentum  $p_R$ , as seen in Fig. 4. This way, for an on-shell resonance a broadening of about 35 MeV at  $\rho_0$  was found in [18].

It is well known from various calculations [19, 20, 21], that the applicability of the low density theorem may be restricted to a regime of rather small densities. In order to overcome this problem we have developed a coupled

channel analysis of the properties of  $\pi$ ,  $\rho$  and  $\eta$  mesons as well as baryon resonances in nuclear matter [9, 20, 22]. The resonance parameters are taken from the analysis of Manley *et al.* [11]. The in-medium propagators of the mesons are determined from the excitation of nucleon-hole and resonance-hole loops. The resonance self energy in nuclear matter  $\Sigma_{\text{med}}$  is obtained by replacing the vacuum meson propagator with the in-medium one in the meson nucleon loops, see Fig. 3. Of course, also the correction from Pauli blocking is included. The collisional broadening is given by:

$$\Gamma_{\text{coll}}(\sqrt{s}, p) = \frac{\text{Im} \Sigma_{\text{med}}(\sqrt{s}, p) - \text{Im} \Sigma_{\text{Pauli}}(\sqrt{s}, p)}{\sqrt{s}}, \quad (12)$$

where  $\text{Im} \Sigma_{\text{Pauli}}$  is the Pauli-blocked vacuum width. By coupling the meson and resonance properties a self-consistency problem arises, which we solve iteratively. The physical interpretation is that higher iterations involve reactions on more than one nucleon. For example, going to the next order effectively takes into account 3-body processes of the resonances. This is clearly beyond the low density theorem.

Concerning the properties of the  $S_{11}$  resonance, we find a net broadening of 35 MeV at  $\rho_0$  for an on-shell resonance. As can be seen in Fig. 4, in the momentum range of interest between 0.6 and 1 GeV this result is in absolute size (relative to the total width at  $\rho_0$ ) close to that of [18]. Effects from the dressing of  $\pi$  and  $\eta$  mesons are of the order of a few MeV, the only sizeable contribution to the collisional broadening coming from the  $N\rho$  sector (for details we refer the reader to [9]). This is in qualitative agreement with the calculation of [23], where a somewhat larger value for the broadening was predicted. The strong in-medium correction in the  $N\rho$  channel is due to the coupling of the  $D_{13}(1520)$  state to the  $\rho$  meson, which moves spectral strength down to smaller invariant masses [20, 22] in the  $\rho$  mass distribution. This way, the phase space available for the decay of a  $S_{11}(1535)$  is enhanced. The slightly different momentum behavior of the collision widths (12) compared to the collision rates (10) is due to the resummation of particle-hole loops in the meson propagators. This leads to a decrease of the  $N\eta$  contribution and an increase of the  $N\rho$  contribution with increasing  $p_R$ , leaving the total width  $\Gamma_{\text{coll}}$  nearly constant. This behavior, however, cannot be extrapolated to very small momenta  $p_R < 0.3$  GeV due to effects from Pauli blocking in the  $N\eta$  channel.

We find that the main effect from the inclusion of higher order effects is a slight reduction of the broadening in the  $N\rho$  channel. This is due to the strong broadening of the  $D_{13}(1520)$  which leads to a moderate reduction of this state in the  $\rho$  spectral function. Therefore, some  $\rho$  spectral strength is moved up to larger invariant masses, and the decay of a  $S_{11}$  to the  $N\rho$  channel is somewhat suppressed.

We have also calculated the mass shift corresponding to the broadening of the  $S_{11}$  by means of a dispersion analysis [9]. As a result we do not observe any significant shift. This, of course, supports the hypothesis, that the mass shift as observed in the photo-nucleus data, see Fig. 5, is due to binding effects, see Section IV. In the actual calculation, we therefore do not include the dispersive mass shift.

The influence of the medium on the  $S_{11}$  enters the calculations in two different ways: The reactions displayed in (9), which are directly connected with a collision rate via Eq. (10), are implemented explicitly in the model. Due to the fact that the results for the collisional width (Eq. (12)) are close to the collision rates, the consistency between the widths and these explicit processes is maintained. Furthermore, since the  $S_{11}$  final states are not restricted to the vacuum decay channels, the width  $\Gamma_{S_{11} \rightarrow X}$  in Eqs. (6) and (8) has to be substituted by the full in-medium width.

#### IV. RESULTS

In Fig. 5 we show our results for the reaction  $\gamma A \rightarrow \eta X$  for different nuclei in comparison with the TAPS and KEK data. The latter are obtained by integration over  $0^\circ \leq \vartheta \leq 90^\circ$ , while the former data as well as our calculations cover the full angular range. However, the main contribution stems from angles smaller than  $90^\circ$ . Imposing this limitation on our calculations, deviations smaller than 3% are found.

The dashed and solid curves in each plot correspond to the two potentials (H) and (M) described in Sec. II. The calculations include Fermi motion, Pauli blocking, nuclear binding effects and FSI, but  $S_{11}$  vacuum widths are used in the cross sections (6) and (8). The dotted curves do involve the full  $S_{11}$  in-medium width in the cross sections and therefore show the total influence of collisional broadening.

The curves (M) are shifted by about 50-70 MeV compared to the curves (H). This can be understood by taking a look at the elementary reaction  $\gamma N \rightarrow S_{11}(1535)$ . The momentum independent potential (H) is identical both for incoming nucleon and outgoing resonance. The resonance mass is obtained from the cm energy  $\sqrt{s}$  (i.e. effective resonance mass) by subtracting the resonance potential:

$$\mu_{\text{H}} = \sqrt{s} - S_{\text{H}}.$$

In the case of the momentum dependent potential (M) we obtain a different result. For photon energies of about 800 MeV the outgoing resonance has also a momentum of about 800 MeV. For such momentum values, the potential (M)

is almost zero, see Fig. 1. Therefore we get for the resonance mass  $\mu_M = \sqrt{s}$ , which is smaller compared to  $\mu_H$ :

$$\mu_M = \sqrt{s} = \mu_H - |S_H|.$$

Hence the peak maxima in both scenarios are shifted relatively to each other by roughly  $|S_H|$ , which is approximately 50-70 MeV.

As one can see, the curves (H) overestimate the TAPS data in the threshold region and exhibit a maximum shifted towards lower energies with respect to the peak maximum suggested by the KEK data. In contrast, the curves (M) only slightly underestimate the TAPS data, but are in very good agreement with the KEK data, especially the location of the peak maximum is well reproduced.

The influence of the collisional broadening of the  $S_{11}$  has only little influence. As can be seen from the dotted curves, which visualize the effect of the medium modification via the cross sections (6) and (8). In order to completely analyze the influence of collisional broadening, we show in Fig. 6 four different szenarios: The dashed curve shows the calculation without any FSI. The dashed-dotted curve includes FSI except for the  $S_{11}$  FSI in (9) and therefore shows the influence of the direct  $\eta$  absorption via resonance re-excitation. Both calculations use vacuum widths in the cross sections (6) and (8). The solid curves include all FSI and corresponds to the solid curves in Fig. 5. The dotted curve also includes the full in-medium widths in the cross sections and corresponds to the dotted curves in Fig. 5. It is seen that the main effect comes from the direct  $\eta$  absorption via  $\eta N \rightarrow R$ , whereas the influence of in-medium effects concerning the  $S_{11}$  is rather small. This is not surprising, because the mean free path  $\lambda$  of a  $S_{11}$  at  $\rho_0$  is about 3 fm – compared to  $\lambda \lesssim 1$  fm for the  $\eta$  – whereas the RMS radius of C is about 2.5 fm. This is in contrast to the results of Yorita *et al.* [2], who find a strong effect from the  $S_{11}$  FSI.

In Fig. 7 we show the effect of the FSI in the case of Calcium. The solid line includes FSI. The dotted curve is the result without FSI divided by a constant factor of 1.9. In both calculations we used the potential (M) and neglected the medium modification of the  $S_{11}$  widths. It is clearly visible that the absorption depends on energy and therefore the assumption of a constant absorption factor made in [4] is unrealistic. This result also holds for other nuclei. On the other hand, the issues raised in [4] concerning the peak position can be verified. The claim there was that the peak position can only be described by assuming vanishing scalar and vector potentials for the  $S_{11}(1535)$ . This scenario is close to what we get with the momentum dependent potential (M) for the  $S_{11}$ , which – as mentioned above – nearly vanishes in the kinematical regime under investigation.

## V. SUMMARY

We have calculated  $\eta$  photoproduction on several nuclei in the energy region dominated by the  $S_{11}(1535)$  resonance. Starting from a parametrization of the data for the elementary  $\gamma N \rightarrow \eta N$  reaction, we applied a BUU transport model to account for final state interactions. The calculations including a momentum dependent potential for the nucleons and the  $S_{11}$  reproduce the available data well. In the threshold region a slight underestimation of the data is observed. The calculations involving a momentum independent potential clearly overestimate the data.

The collisional width of the  $S_{11}$ , calculated within a realistic self-consistent resonance-hole model [9], was found to be close to the collision rates from [18] and was included in the transport calculations. The influence of collisional reactions of the  $S_{11}$  on the cross section were found to be small, in contrast to the QMD calculations of Yorita *et al.* [2]. The main difference between the result without FSI and the full calculation can be attributed to the absorption of the  $\eta$  in the FSI e.g. via  $\eta N \rightarrow S_{11} \rightarrow \pi N$ . Finally, we have shown that the absorption reactions cannot be mimicked by applying a constant factor to the results without FSI.

## ACKNOWLEDGMENTS

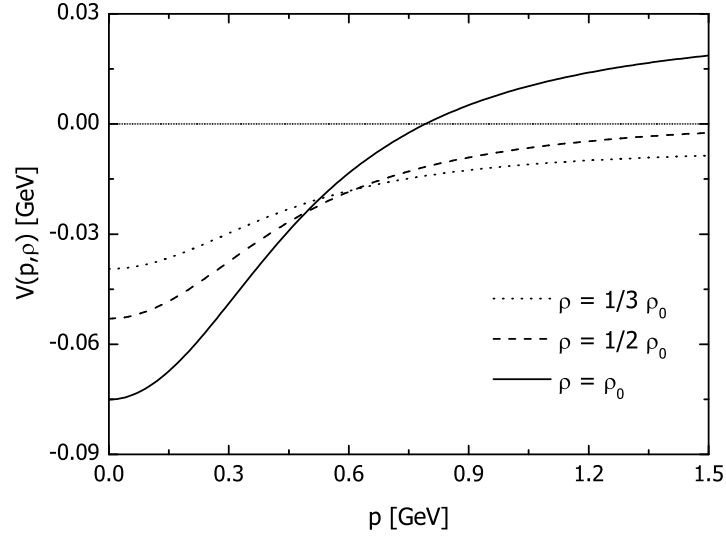
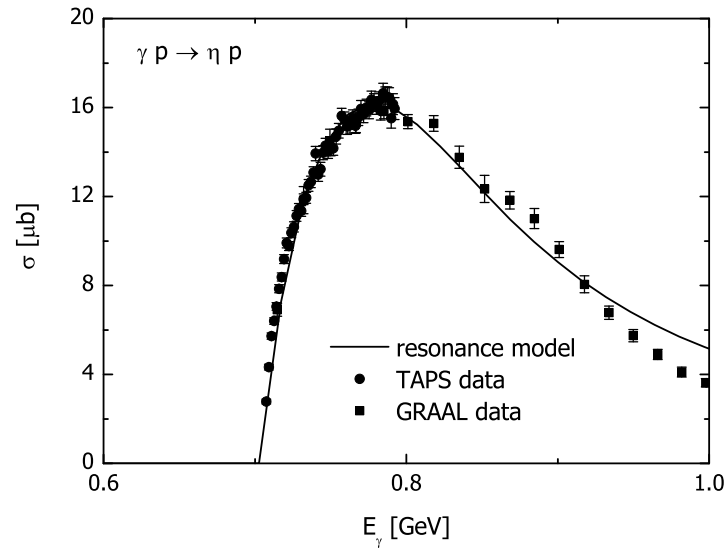
This work was supported by DFG.

- 
- [1] M. Rößig-Landau *et al.*, Phys. Lett. **B373**, 45 (1996).
  - [2] T. Yorita *et al.*, Phys. Lett. **B476**, 226 (2000).
  - [3] H. Yamazaki *et al.*, Nucl. Phys. **A670**, 202c (2000).
  - [4] T. Maruyama and S. Chiba, nucl-th/0204051.
  - [5] S. Teis, W. Cassing, M. Effenberger, A. Hombach and U. Mosel, Z. Phys. **A356**, 421 (1997).
  - [6] M. Effenberger, A. Hombach, S. Teis and U. Mosel, Nucl. Phys. **A614**, 501 (1997).

- [7] J. Lehr, M. Effenberger and U. Mosel, Nucl. Phys. **A671**, 503 (2000).
- [8] A. Hombach, A. Engel, S. Teis, U. Mosel, Z. Phys. **A 352**, 223 (1995).
- [9] M. Post, in preparation.
- [10] M. Effenberger, E. Bratkovskaya and U. Mosel, Phys. Rev. **C60**, 044614 (1999).
- [11] D.M. Manley and E.M. Saleski, Phys. Rev. **D45**, 4002 (1992).
- [12] C. Gale, G. Welke, M. Prakash, S. Lee and S. Das Gupta, Phys. Rev. **C41**, 1545 (1990);  
G. Welke, M. Prakash, T. Kuo and S. Das Gupta, Phys. Rev. **C38**, 2101 (1988).
- [13] G. Penner, U. Mosel, Phys. Rev **C66**, 055212 (2002).
- [14] R. L. Walker, Phys. Rev. **182**, 1729 (1969).
- [15] B. Krusche *et al.*, Phys. Rev. Lett. **74**, 3736 (1995).
- [16] B. Krusche *et al.*, Phys. Lett. **B358**, 40 (1995).
- [17] F. Renard *et al.*, Phys. Lett. **B528**, 215 (2002).
- [18] M. Effenberger, A. Hombach, S. Teis and U. Mosel, Nucl. Phys. **A613**, 353 (1997).
- [19] E. Oset and L.L. Salcedo, Nucl. Phys. **A468**, 631 (1993).
- [20] W. Peters, M. Post, S. Leupold, H. Lenske and U. Mosel, Nucl. Phys. **A632**, 109 (1998).
- [21] M.F.M. Lutz and E.E. Kolomeitsev, Nucl. Phys. **A700**, 193 (2002).
- [22] M. Post, S. Leupold and U. Mosel, Nucl. Phys. **A689**, 753 (2001).
- [23] H. C. Chiang, E. Oset and L. C. Liu, Phys. Rev. **C44**, 738 (1991) .

TABLE I: Parameters for the mean-field potential  $V$ .

	incompressibility [MeV]	$A$ [MeV]	$B$ [MeV]	$C$ [MeV]	$\tau$	$\Lambda$ [ $\text{fm}^{-1}$ ]
H	380	-124.3	71.0	0.	2.0	-
M	290	-29.3	57.2	-63.5	1.76	2.13

FIG. 1: Momentum dependence of the potential  $V$  with parameter set (M) given in Tab. I for different densitiesFIG. 2: Parametrization of the elementary process  $\gamma p \rightarrow \eta p$  according to Eq. (6). The data are taken from [15] and [17].

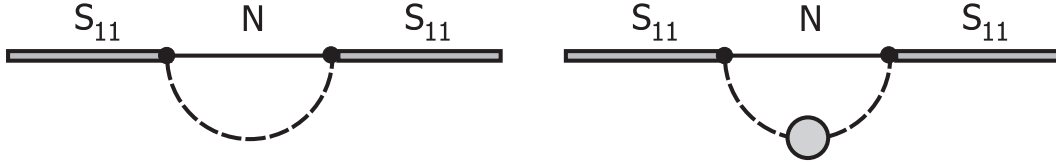


FIG. 3: Feynman diagram for the self energy of the  $S_{11}$  resonance in vacuum (left) and in nuclear matter (right). The dashed line represents the exchange of  $\pi$ ,  $\eta$  or  $\rho$  mesons. By the blob in the meson line the full in-medium propagator for the mesons, which are dressed by the excitation of nucleon-hole and resonance-hole loops, is indicated.

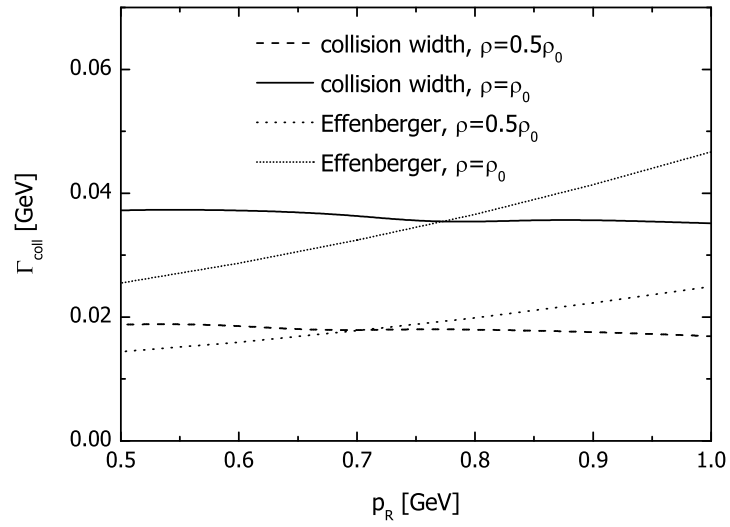


FIG. 4:  $S_{11}$  collision width at the pole mass as a function of the resonance momentum  $p_R$  for different densities (dashed and solid curves). Also shown are the results of Effenberger *et al.* [18] (dotted curves).

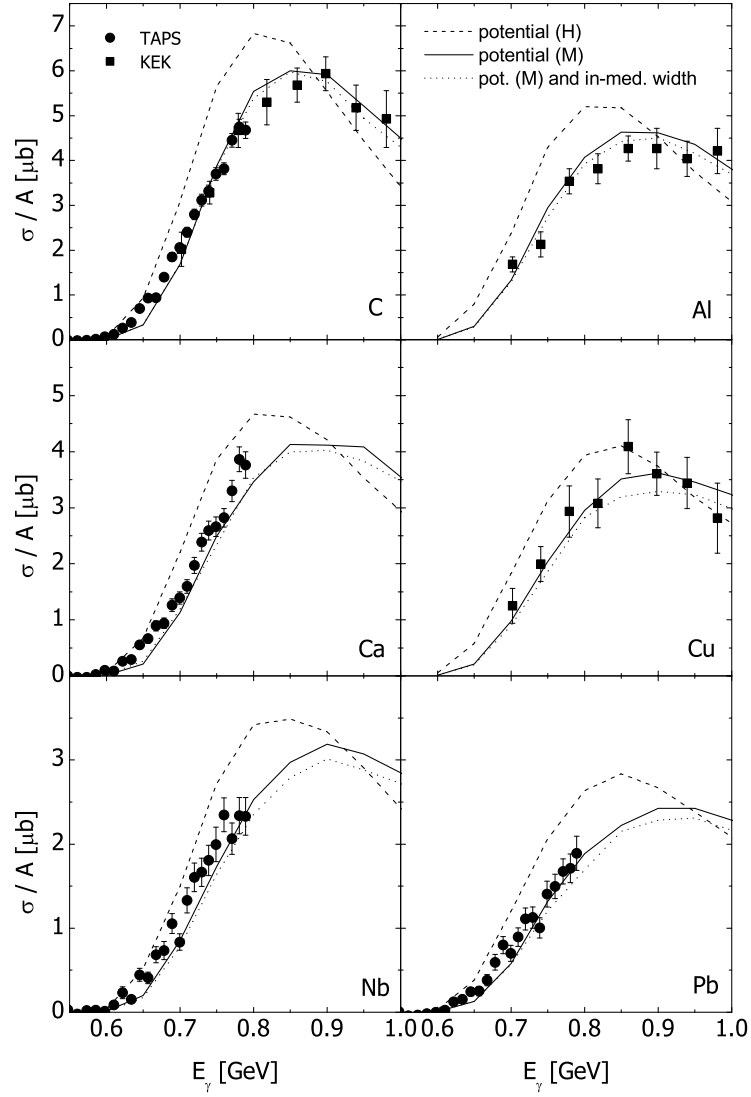


FIG. 5: Results of the BUU model for the reaction  $\gamma A \rightarrow \eta X$  on different nuclei. The dashed and solid lines correspond to the usage of the potentials (H) and (M). The dotted lines include the medium-modified width for the  $S_{11}(1535)$  discussed in Sec. III. The data are from [1] (circles) and [2, 3] (squares).

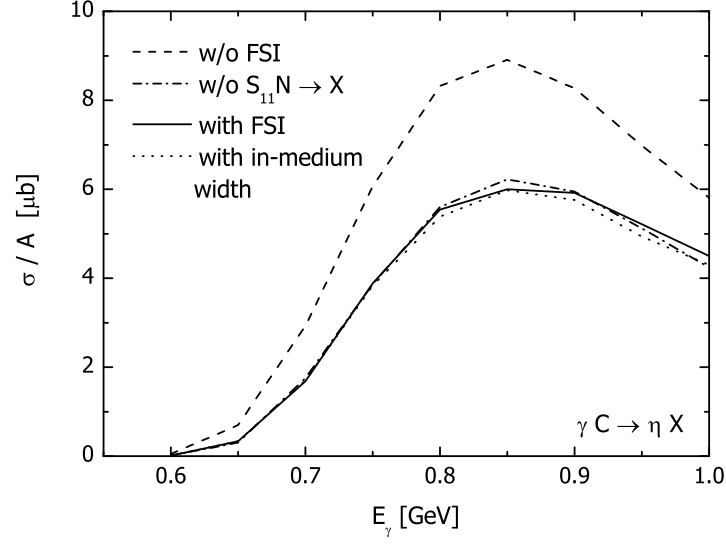


FIG. 6: Influence of medium modifications on  $\eta$  photoproduction on Carbon with potential (M). The dashed curve shows the result without FSI, the dashed-dotted includes FSI except for the  $S_{11}$  collision reactions. The solid curve includes all FSI and vacuum widths in the cross section for the  $S_{11}$  excitation and corresponds to the solid line in Fig. 5. The dotted curve includes full in-medium widths in these cross sections and coincides with the dotted curve in Fig. 5.

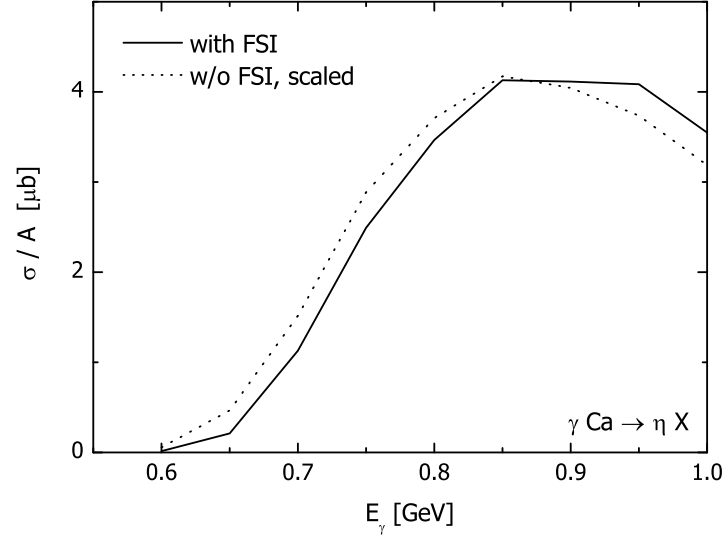


FIG. 7: Influence of the FSI on the cross section  $\gamma\text{Ca} \rightarrow \eta X$ . The solid curve shows the result with FSI, while the dotted line is the result without FSI divided by a factor of 1.9. All curves include the potential (M). In-medium modifications of the  $S_{11}$  width are neglected.